Two-dimensional localized chaotic patterns in parametrically driven systems

Deterlino Urzagasti[1], David Laroze[2,3],* and Harald Pleiner[3]
[1]*Instituto de Investigaciones Físicas, UMSA, P.O. Box 8635, La Paz, Bolivia*
[2]*Instituto de Alta de Investigación, CEDENNA, Universidad de Tarapacá, Casilla 7D, Arica, Chile. and*
[3]*Max Planck Institute for Polymer Research, D 55021 Mainz, Germany.*
(Received 26 January 2017; published 25 May 2017)

We study two-dimensional localized patterns in weakly dissipative systems that are driven parametrically. As a generic model for many different physical situations we use a generalized nonlinear Schrödinger equation that contains parametric forcing, damping, and spatial coupling. The latter allows for the existence of localized pattern states, where a finite-amplitude uniform state coexists with an inhomogeneous one. In particular, we study numerically two-dimensional patterns. Increasing the driving forces, first the localized pattern dynamics is regular, becomes chaotic for stronger driving and finally extends in area to cover almost the whole system. In parallel, the spatial structure of the localized states becomes more and more irregular ending up as a full spatiotemporal chaotic structure.

DOI: 10.1103/PhysRevE.95.052216 PACS: 75.78.Fg,85.75.-d,89.75.Kd

I. INTRODUCTION

Dynamic systems that are driven out of equilibrium can show different states, which in the long-time, asymptotic limit can be regular (e.g. stationary, periodic or quasiperiodic) or chaotic. In space, those states are either homogeneous or show a pattern [1]. Nonequilibrium allows for the coexistence of such phases within a broad range of material parameters that characterize the peculiar system under consideration. In particular, one can find localized states, where one state occupies only a restricted spatial area, while another one fills the rest of the space. If the latter is uniform and the former a pattern, the structure is called a localized pattern.

Here we are interested in localized chaotic patterns, where the pattern state in the restricted area is chaotic. Such states have attracted much attention from both, the experimental [2–6] and theoretical [7–17] points of view. We concentrate on parametrically driven *weakly dissipative systems* [18], i.e., genuine time-reversible systems that are only slightly perturbed by the injection and energy dissipation due to the driving. Among them are parametrically driven nonlinear lattices, pulse propagation in nonlinear optical fibers, phase-sensitive optical amplifiers, magnetization waves in easy-plane ferromagnets subject to an oscillatory magnetic field, Faraday-vibrated damped coupled nonlinear pendula chains, liquid crystalline lightvalves with optical feedback, convection in binary mixtures, magnetic fluids, and others [19–27].

Those systems typically show patterns, and in particular localized patterns, close to the bifurcation, where the parametrically driving field is in subharmonic resonance with the system's dynamics. A generic model for the theoretical description serves an amplitude equation derived by the standard weakly nonlinear stability analysis [28]. In lowest order of the expansion involved the parametrically driven damped nonlinear Schrödinger (PDDNLS) equation [29] is obtained. It has been used to discuss, e.g., soliton-like solutions [30–32], two-soliton states [33, 34], and spatiotemporal chaos [35]. However, it only allows for the coexistence of a pattern state with the trivial, zero-amplitude state [36], but not with a uniform, finite amplitude one [37–41], which is the prerequisite [42, 43] for the existence of localized states of the kind we are interested in. For their description the expansion has to be continued to the next order, resulting in the generalized parametrically driven damped nonlinear Schrödinger (gPDDNLS) equation [37].

Recently, we used this equation to study [44] localized chaotic patterns close to the subharmonic bifurcation. Those patterns are found to be generally one dimensional. In this article, we report the finding of chaotic structures that are localized in two dimensions.

In the following we first present the underlying amplitude equation in dimensionless form and discuss where localized states can be expected. We then discuss the numerical methods and tools that allow us to get and characterize those states. Finally we show the numerical results, in particular the two-dimensional (2D)-localized chaotic states, which, as a nontrivial result, are stable even in two dimensions. The paper is arranged as follows: In Sec. II the theoretical model is presented, and in Sec. III numerical simulations are performed and the results are discussed. Finally, conclusions are given in Sec. IV.

II. THEORETICAL MODEL

We employ the gPDDNLS equation for the dimensionless two-dimensional amplitude, $A = A(x, y, t)$, the en-

* corresponding author: dlarozen@uta.cl

velope of the underlying oscillations of the system. Using suitable dimensionless space and time coordinates it takes the form

$$\begin{aligned}\frac{\partial A}{\partial t} &= -i\nu A - i|A|^2A - i\nabla^2 A - \mu A + \gamma A^* \\ &+\gamma\left\{b|A|^4A^* + \delta A^3 + \beta|A|^2A^3 + \alpha|A|^2A^*\right\} \\ &+ia|A|^4A + \kappa\nabla^2 A - c|A|^2A, \end{aligned} \quad (1)$$

containing (in the first line) detuning, the distance of the frequency of the external driving to the subharmonic resonance (ν), cubic saturation, dispersion, linear damping (μ), and external linear driving (γ), with A^* the complex conjugate of A and $\nabla^2 f = \partial^2 f/\partial x^2 + \partial^2 f/\partial y^2$. Nonlinear parametric forcing ($\sim b, \delta, \beta, \alpha$) and quintic saturation (a), diffusion (κ), nonlinear damping (c) are described in the second and third line, respectively. This equation has, e.g. the trivial solution, $A = 0$, corresponding to no oscillations of the underlying physical system, and $A = const.$ describing a (non-trivial) homogeneous and steady oscillation.

The first line of Eq. (1) constitutes the PDDNLS equation, which reduces for $\mu = 0 = \gamma$ to the standard nonlinear Schrödinger equation that is used to describe Hamiltonian equilibrium systems [45]. For the PDDNLS equation the trivial, zero amplitude solution is always (linearly) stable. In fact, stable localized states that connect asymptotically to the zero background solution were found in Ref. [36]. Nevertheless, the constant nontrivial solutions are unstable, due to the spatial coupling, $\sim i\nabla^2 A$ [37]. Therefore, PDDNLS cannot describe (chaotic) localized patterns that are asymptotically connected with nontrivial homogeneous solutions.

Another generalization of the PDDNLS equation that leads to stable homogeneous oscillating states is the complexification of its parameters producing a parametrically driven complex Ginzburg-Landau model [46–48]. Other generalizations applied to intrinsic localized modes in parametrically driven arrays of nonlinear resonators can be found in Ref. [49].

The gPDDNLS Eq. (1) allows for stable nontrivial homogeneous solutions. Not all of the additional terms are necessary to obtain this goal and we choose $\kappa = 0 = c$ (some effects of those parameters have been discussed in [46–49]). The nontrivial homogeneous amplitude states bifurcate from $A = 0$ at $\gamma^2 = \mu^2 + \nu^2$, which defines the so-called first Arnold tongue in the $\gamma - \nu$ parameter space. The stability of these states for a wide range of parameters can be established numerically. Their stability allows for generating localized states that connect one homogeneous state with other homogeneous one. For example, connecting the zero state with a nontrivial one leads to kink patterns [46]; connecting two different nontrivial states gives pulses [37].

In addition, the gPDDNLS Eq. (1) shows spatially inhomogeneous solutions, depicting extended or (one-dimensional) localized patterns. It can be shown analytically [44, 47] that they bifurcate via a finite amplitude instability from the ground state within the Arnold tongue, for $\gamma^2 > \mu^2 + \nu^2$ and $\nu < 0$. These pattern states are stable and undergo, when the driving γ is increased, multiple bifurcations from being stationary (in time) to oscillatory and finally to chaotic behavior. This is also found by numerical investigations. In the following we show numerically that in this region of the parameter space also two-dimensional, in particular chaotic, localized patterns exist and are stable.

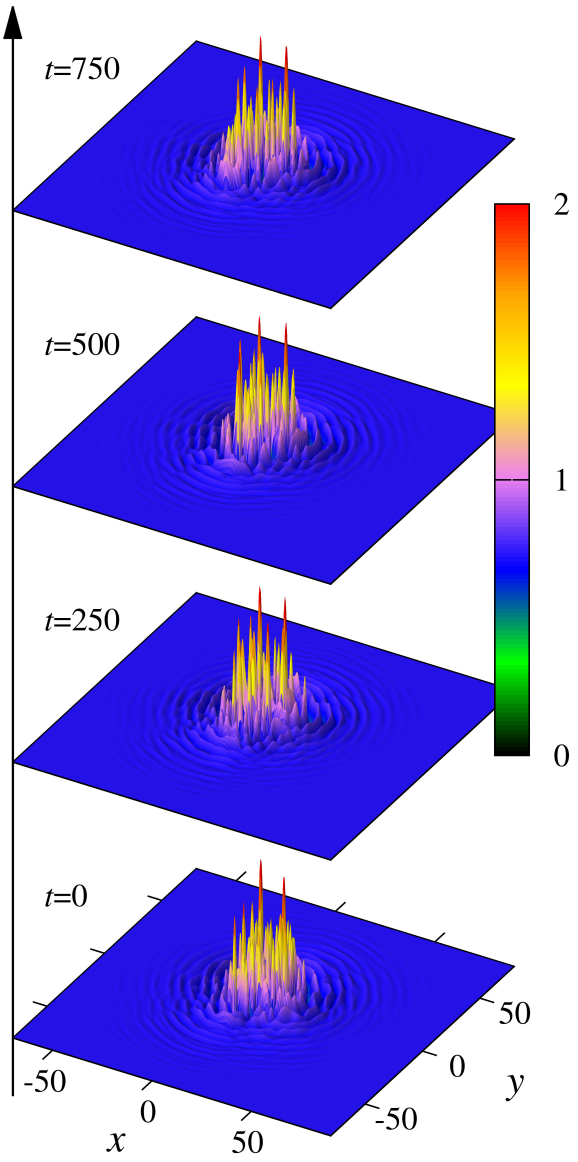

FIG. 1. Evolution of $|A(x, y, t)|$, color-coded on the right, for a chaotic localized pattern at $\gamma = 0.9$ after an initial time interval $\Delta t = 5.6 \times 10^3$ has elapsed. Note the blue, nonzero background.

III. NUMERICAL SIMULATIONS

To solve numerically the amplitude equation, Eq. (1), we use a fifth-order Runge-Kutta scheme with variable step length for the time evolution and a sixth-order central finite-difference method to approximate the spatial derivatives over the system's area $2L \times 2L$. Here we consider $L = 100$ and use 500×500 points, which implies

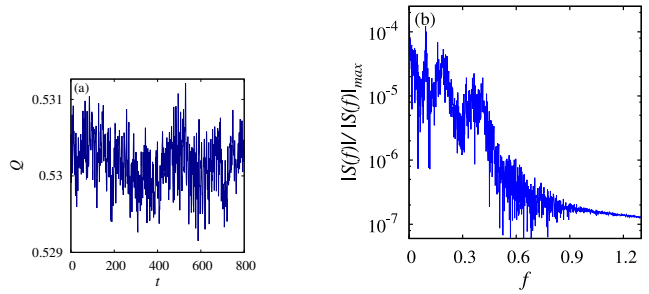

FIG. 2. Energy function Q of a chaotic localized two-dimensional pattern, as a function of (a) time and (b) its corresponding Fourier power spectrum at $\gamma = 0.9$, after a time interval $\Delta t = 5.6 \times 10^3$ has elapsed.

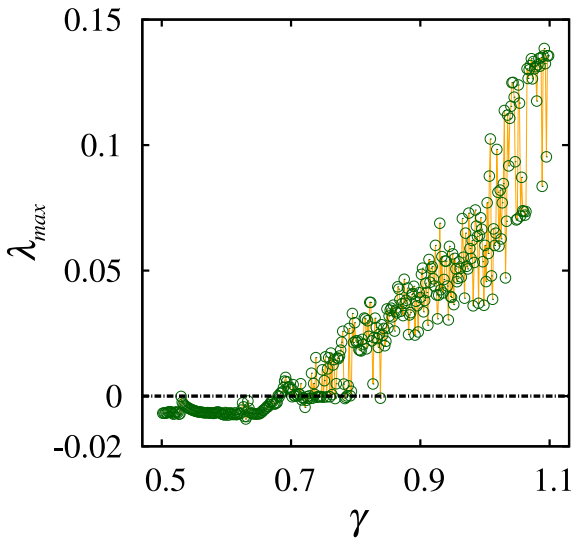

FIG. 3. Largest Lyapunov exponent as a function of γ at $\nu = -0.05$.

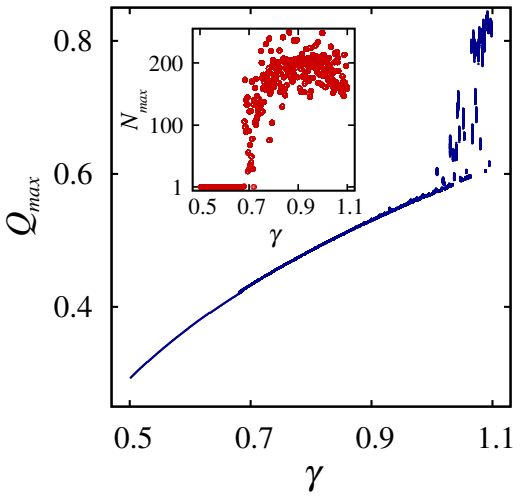

FIG. 4. Bifurcation diagram of Q_{max} as a function of γ. The inset represents the number of different values of Q_{max}.

$\Delta x = \Delta y = 200/500 = 0.4$. We use a double precision Runge-Kutta method described in Ref. [50], which admits the error tolerance to be chosen and which we set as 10^{-7}. We use von-Neumann boundary conditions. We have also checked smaller and larger area sizes to guarantee that there are no finite size effects for $L = 100$. After any temporal transients have faded away we have continued the calculations for at least twice the full transient time with a maximum integration time $t = 8.0 \times 10^3$.

We essentially characterize the different types of dynamical behavior of the system by the energy function Q, the statistical width of the localized pattern Δ, and the largest Lyapunov exponent of the evolving dynamics, λ_{max}. The first one is the norm of the amplitude defined by

$$Q(t) = \left(\frac{1}{2L}\right)^2 \int_{-L}^{L}\int_{-L}^{L} |A(t,x,y)|^2 \,\mathrm{d}x\mathrm{d}y, \qquad (2)$$

which is often used for the characterization of nonregular dynamics in optics [9–12], localized patterns in fluids, and other physical systems [27, 51]. Q is generally a function of time reflecting the temporal information of the patterns, i.e. in a stationary, (quasi-) periodic, or chaotic regime,$Q(t)$, too, is constant, (quasi-) periodic, or chaotic, respectively. To identify the different temporal regimes, we calculate its power spectrum $|S(f)|$ in frequency space f.

A more quantitative aspect of the dynamics is provided by the largest Lyapunov exponent, λ_{max}, [52], defined by

$$\lambda_{max} = \lim_{t\to\infty} \frac{1}{t} \ln \frac{\|\delta A(t,x,y)\|}{\|\delta A(t_0,x,y)\|}, \qquad (3)$$

where $\|\bullet\| \equiv (\int_{-L}^{L}\int_{-L}^{L} |\bullet|^2 \,\mathrm{d}x\mathrm{d}y)^{1/2}$ and δA is a four-dimensional vector field that satisfies the differential equation

$$\frac{\partial \delta A}{\partial t} = \bar{\mathbf{J}} \cdot \partial A, \qquad (4)$$

with $\bar{\mathbf{J}}$ the Jacobian matrix of Eq. (1) with respect to A. Although Eq. (4) is linear with respect to δA, it depends on A due to the nonlinear terms in Eq. (1). Hence, to calculate the Lyapunov exponent one needs to solve the coupled system given by Eqs. (1) and (4).

The number λ_{max} quantifies how fast the distance, δA, between two initially close trajectories of the field A either vanishes ($\lambda_{max} < 0$) or diverges exponentially ($\lambda_{max} > 0$). The latter is the hallmark of chaotic behavior. We have calculated λ_{max} from $t_0 = 5.6 \times 10^3$ up to $t_{max} = 8.0 \times 10^3$. In order to overcome exponential divergences we rescale $\|\delta A(t,x,y)\|$ by the initial norm $\|\delta A(t_0,x,y)\|$ and take as time steps $\Delta t = 800/1024 = 0.78125$. This method has been extensively used for many different dynamical systems to quantify chaos [52–58] and also allows to discriminate between quasiperiodic and chaotic dynamics.

For the analysis of the spatial patterns we compute first the normalized moment $\Sigma = <x^2 + y^2> - <x>^2 - <y>^2$ with $|A(t,x,y)|^2$ as the statistical weight. We

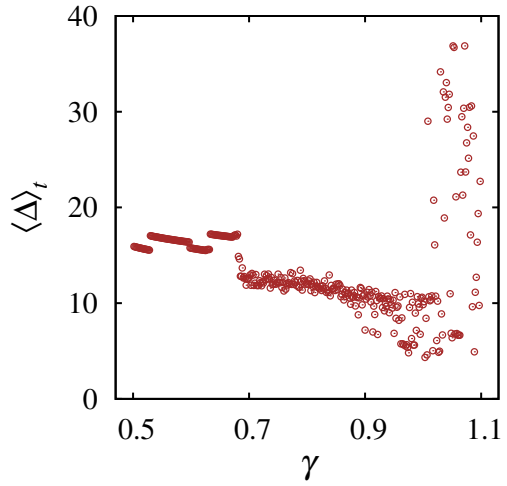

FIG. 5. Time average of the width, $< \Delta >_t$, as a function of γ.

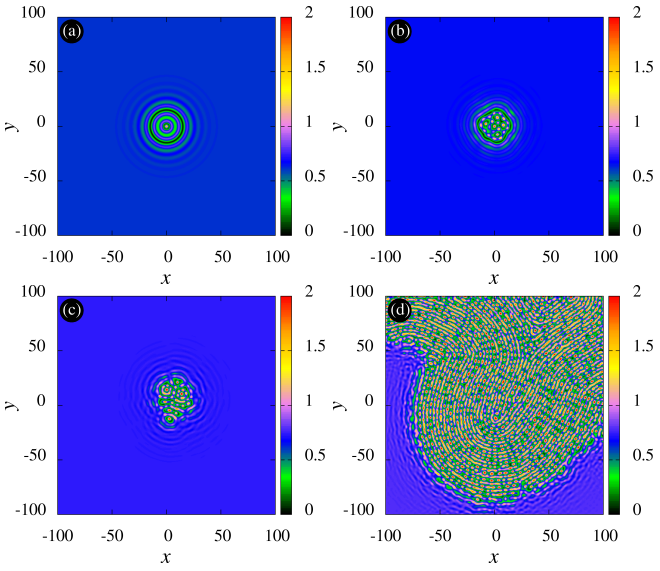

FIG. 6. A snapshot at $t = 5.6 \times 10^3$ of $|A|$ for localized and extended patterns at different values of γ: for $\gamma = 0.6$ a localized stationary one with $\lambda_{max} = -0.007$ (upper left), for $\gamma = 0.7$ a localized quasiperiodic one with $\lambda_{max} = 0.000$ (upper right); for $\gamma = 0.9$ a localized chaotic one with $\lambda_{max} = 0.049$ (lower left), and for $\gamma = 1.1$ an extended chaotic one with $\lambda_{max} = 0.134$ (lower right). Videos can be found in the Supplemental Material [59] for $\gamma = 0.7$ and 0.9.

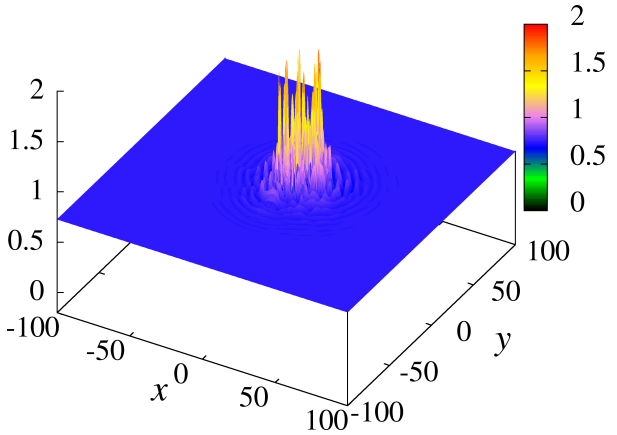

FIG. 7. Three-dimensional representation of the localized chaotic structure at $\gamma = 0.9$, shown in the lower left part of Fig. 6. Appropriate videos can be found in the Supplemental Material [59].

then use $\Delta = 2|\Sigma - \Sigma_c|^{1/2}$ as a measure for the width of the localized pattern, where $\Sigma_c = (2/3)L^2$ is the moment for a stationary state with $A = \text{const}$. The time-averaged $< \Delta >_t$ is used below to present the spatial aspects of the results.

In this article, we concentrate the discussion on the influence of the driving force. Fixing the detuning to $\nu = -0.05$ in order to scan the appropriate parameter space region, we use the driving force coefficient, γ, as the bifurcation parameter. For the material properties we choose $\mu = 0.35$, $b = 1/12$, $\delta = 4/15$, $\beta = -1/24$, $\alpha = -0.65$, and $a = 1/6$, since for those values an experimental realization might be possible. For a pendula chain system similar values can be derived [37–39].

The central result we want to report in this article is shown in Fig. 1: a chaotic structure that is localized in two dimensions. The values of $|A(x, y)|$ for four different fixed times (horizontal planes) is depicted using the color code on the right. The blue areas outside the localized structure have a constant, nonzero amplitude. The irregular behavior in time is obvious. To be more precise we show the energy function $Q(t)$, Eq. (2), for a long time period and the resulting Fourier spectrum in Fig. 2. Both show the typical behavior of chaotic time sequences.

This is corroborated by the largest Lyapunov exponent shown in Fig. 3. For a driving force parameter $\gamma = 0.9$ used in the previous figures, λ_{max} is positive, indicating chaos. There is a kind of transition at around $\gamma = 0.7$, below which λ_{max} is negative and the behavior regular. Above, λ_{max} generally is positive. However, there are still some special values of γ, where $\lambda_{max} = 0$, and the system is quasiperiodic. Such islands become sparse and finally disappear, when γ is increased further. For $\gamma \gtrsim 1.0$ another change in the behavior [in the average slope of $\lambda_{max}(\gamma)$] can be seen. Matching information is gained from the maximum values of $Q(t)$ that can be found within a given time interval. In the periodic case all maxima found are equal and only one value for Q_{max} is found. This is the case for $\gamma < 0.7$ in Fig. 4, where $Q_{max}(\gamma)$ is a smoothly increasing line. In the chaotic (and quasiperiodic) regime, many maxima exist as is shown in the inset of that figure. They have different values of Q_{max} showing up in Fig. 4 as a band of finite width. Again, for $\gamma \gtrsim 1.0$ a dramatic change in the behavior is seen.

Further understanding of this localized chaotic structure is obtained by considering the spatial structure. Figure 5 shows the time-averaged width of the pattern as a function of the driving. In the regime of regular dynamics the averaged size of the pattern is generally a smooth function of the driving, only interspersed by a few well-defined jumps. In the time-chaotic regime

also the averaged width changes rather abruptly with the driving force, while in the final regime at $\gamma \gtrsim 1.0$ the pattern grows dramatically, but in a strongly erratic manner. The appropriate patterns for the different regimes are shown as snapshots in Fig. 6. The regular dynamics refers to a regular ring structure (upper left frame). Since the mean width slightly decreases with increasing driving force, an additional ring is added for a few special values of the driving force giving rise to the jumps shown in Fig. 5. When the dynamics of the localized pattern is chaotic, also the spatial structure is irregular (lower left frame). This is obvious from Fig. 7, which depicts this case, not only by characterizing the values of the amplitude $|A|$ by colors, but also by spikes of different height. We mention that this localized chaotic solution grows rapidly into an extended one, if the PDDNLS equation is used instead of the gPDDNLS one, (cf. Supplemental Material [59]).

The combination of temporal chaos and spatial irregularity into spatiotemporal chaos is best viewed in the videos (for $\gamma = 0.7$ and 0.9) in the Supplemental Material [59]. The transition from a localized to an extended (chaotic) pattern for very strong driving is demonstrated in the lower right frame of Fig. 6.

IV. CONCLUSIONS

Spatiotemporal localized structures are found in a *two-dimensional* dissipative parametrically driven system. The prototype model is a generalization of the parametrically driven damped nonlinear Schrödinger equation, which describes parametric instabilities in fluids, granular materials, optical devices, nonlinear pendulum chains, as well as in magnetic systems. Hence, we expect that such two-dimensional localized states can be found in a wide range of physical systems. The various possible states are characterized by Lyapunov exponents and bifurcation diagrams. With increasing driving parameter we first find stationary localized states, and (a small range of) quasiperiodic ones, while above a threshold also chaotic localized states are obtained. Finally, the latter gradually extend in space and become extended states for very large driving parameters.

ACKNOWLEDGMENTS

The authors acknowledge partial support from FONDECYT Grant No. 1120764, CONICYT ANILLO ACT 1410 and center of excellence with BASAL/CONICYT financing, Grant No. FB0807, CEDENNA.

[1] M. C. Cross and P. C. Hohenberg, Rev. Mod. Phys. **65**, 851 (1993).
[2] C. Weizhong, W. Rongjue, and W. Benren, Phys. Rev. E **53**, 6016 (1996).
[3] K. E. Daniels, B. B. Plapp, and E. Bodenschatz, Phys. Rev. Lett. **84**, 5320 (2000).
[4] A. B. Ustinov, V. E. Demidov, A. V. Kondrashov, B. A. Kalinikos, and S. O. Demokritov, Phys. Rev. Lett. **106**, 017201 (2011).
[5] Z. Wang , A. Hagerstrom, J. Q. Anderson, W. Tong, M. Wu, L. D. Carr, R. Eykholt, and B. A. Kalinikos, Phys. Rev. Lett. **107**, 114102 (2011).
[6] N. Verschueren, U. Bortolozzo, M. G. Clerc, and S. Residori, Phys. Rev. Lett. **110**, 104101 (2013).
[7] B. A. Malomed, D. F. Parker, and N. F. Smyth, Phys. Rev. E **48**, 1418 (1993)
[8] R. J. Deissler and H. R. Brand, Phys. Rev. Lett. **74**, 4847 (1995).
[9] N. Akhmediev, J. M. Soto-Crespo, and G. Town, Phys. Rev. E **63**, 056602 (2001).
[10] J. M. Soto-Crespo and N. Akhmediev, Phys. Rev. Lett. **95**, 024101 (2005).
[11] J. M. Soto-Crespo, Ph. Grelu, N. Akhmediev, and N. Devine, Phys. Rev. E **75**, 016613 (2007).
[12] A. Ankiewicz, N. Devine, N. Akhmediev, and J. M. Soto-Crespo, Phys. Rev. A **77**, 033840 (2008).
[13] D. Turaev, M. Radziunas, and A. G. Vladimirov, Phys. Rev. E **77**, 065201 (2011).
[14] Y. Azizi and A. Valizadeh, Phys. Rev. A **83**, 013614 (2011).
[15] Y. V. Kartashov, B. A. Malomed, and L. Torner, Rev. Mod. Phys. **83**, 247 (2011).
[16] O. Descalzi, C. Cartes, J. Cisternas, and H. R. Brand, Phys. Rev. **E** 83, 056214 (2011).
[17] C. Cartes, O. Descalzi, and H. R. Brand Phys. Rev. E **85**, 015205 (2012).
[18] M. Clerc, P. Coullet, and E. Tirapegui, Phys. Rev. Lett. **83**, 3820 (1999).
[19] B. Denardo, B. Galvin, A. Greenfield, A. Larraza, S. Putterman, and W. Wright, Phys. Rev. Lett. **68**, 1730 (1992).
[20] J. N. Kutz, W. L. Kath, R.-D. Li, and P. Kumar, Opt. Lett. **18**, 802 (1993).
[21] S. Longhi, Phys. Rev. E **53**, 5520 (1996).
[22] M. G. Clerc, S. Coulibaly, and D. Laroze, Europhys. Lett. **90**, 38005 (2010).
[23] N. V. Alexeeva, I. V. Barashenkov, and G. P. Tsironis, Phys. Rev. Lett. **84**, 3053 (2000).
[24] I. V. Barashenkov and E. V. Zemlyanaya, Phys. Rev. Lett. **83**, 2568 (1999).
[25] E. V. Zemlyanaya and N. V. Alexeeva, Theor. Math. Phys. **159**, 870 (2009).
[26] N. Verschueren, U. Bortolozzo, M.G. Clerk. and S. Residori, Phil. Trans. R. Soc. **A 372**, 20140011 (2014).
[27] O. Batiste, E. Knobloch, A. Alonso, and I. Mercader, J. Fluid Mech. **560**, 149 (2006).
[28] A. C. Newell and J. A. Whitehead, J. Fluid Mech. **28**, 279 (1969).
[29] J. W. Miles, J. Fluid Mech. **148**, 451 (1984).
[30] D. Urzagasti, D. Laroze, M. G. Clerc, and H. Pleiner, Europhys. Lett. **104**, 40001 (2013).
[31] I. V. Barashenkov, E. V. Zemlyanaya, and T. C. van Heerden, Phys. Rev. E **83**, 056609 (2011).
[32] I. V. Barashenkov, M. M. Bogdan, and V. I. Korobov, Europhys. Lett. **15**, 113 (1991).
[33] D. Urzagasti, D. Laroze, M. G. Clerc, S. Coulibaly, and H. Pleiner, J. Appl. Phys. **111**, 07D111 (2012).
[34] I. V. Barashenkov and E. V. Zemlyanaya, Phys. Rev. E

83, 056610 (2011).
[35] V. S. Shchesnovich and I. V. Barashenkov, Physica D **164**, 83 (2002).
[36] I. V. Barashenkov, N. V. Alexeeva, and E. V. Zemlyanaya, Phys. Rev. Lett. **89**, 104101 (2002).
[37] M. G. Clerc, S. Coulibaly, and D. Laroze, Phys. Rev. E **77**, 056209 (2008).
[38] M. G. Clerc, S. Coulibaly, and D. Laroze, Int. J. Bif. Chaos **19**, 2717 (2009).
[39] M. G. Clerc, S. Coulibaly, and D. Laroze, Int. J. Bif. Chaos **19**, 3525 (2009).
[40] M. G. Clerc, S. Coulibaly, and D. Laroze, Physica D **239**, 72 (2010).
[41] M. G. Clerc, S. Coulibaly, and D. Laroze, Europhys. Lett. **97**, 30006 (2012).
[42] W. van Saarloos and P. C. Hohenberg, Phys. Rev. Lett. **64**, 749 (1990).
[43] P. Coullet, Int. J. Bif. Chaos **12**, 245 (2002).
[44] D. Urzagasti, D. Laroze, and H. Pleiner, Eur. Phys. J. ST **223**, 141 (2014).
[45] C. Sulem and P. L. Sulem, *The Nonlinear Schrödinger Equation: Self-Focusing and Wave Collapse* (Springer-Verlag, NY, 1999).
[46] I. V. Barashenkov, S. Cross, and B. A. Malomed, Phys. Rev. E **68**, 056605 (2003).
[47] J. Burke, A. Yochelis, and E. Knobloch, SIAM J. Appl. Dyn. Sys. **7**, 651 (2008).
[48] Y.-P. Ma, J. Burke, and E. Knobloch, Physica D **239**, 1867 (2010).
[49] E. Kenig, B. A. Malomed, M. C. Cross, and R. Lifshitz, Phys. Rev. E **80**, 046202 (2009).
[50] W. H. Press, S. A. Teukolsky, W. T. Vetterling, and B. P. Flannery. *Numerical Recipes in FORTRAN* (Cambridge University Press, UK, 1992).
[51] J. Burke and E. Knobloch, Chaos **17**, 037102 (2007).
[52] A. Wolf, J. B. Swift, H. L. Swinney, and J. A. Vastano, Physica D **16**, 285 (1985).
[53] J. P. Eckmann, D. Ruelle, and S. Ciliberto, Phys. Rev. A **34**, 4971 (1986).
[54] K. Geist, U. Parlitz, and W. Lauterborn, Prog. Theor. Phys. **83**, 875 (1990).
[55] J. D. Scheel and M. C. Cross, Phys. Rev. E **74**, 066301 (2006).
[56] A. Karimi, and M. R. Paul, Phys. Rev. E **85**, 046201 (2012)
[57] D. Laroze, P.G . Siddheshwar, and H. Pleiner, Commun. Nonlinear Sci. Numer. Simulat. **18**, 2436 (2013).
[58] D. Laroze, and H. Pleiner, Commun. Nonlinear Sci. Numer. Simulat. **26**, 167 (2015).
[59] See Supplemental Material for videos of the localized chaotic structures and for pictures that show the delocalization, if the conventional PDDNLS equation is used.